

# QMRTTools: a Mathematica toolbox for quantitative MRI analysis.

Martijn Froeling<sup>1</sup>

DOI: [10.21105/joss.01204](https://doi.org/10.21105/joss.01204)

## Software

- [Review ↗](#)
- [Repository ↗](#)
- [Archive ↗](#)

Submitted: 04 January 2019

Published: 11 June 2019

## License

Authors of papers retain copyright and release the work under a Creative Commons Attribution 4.0 International License ([CC-BY](#)).

## Summary

QMRTTools is written in Mathematica using Wolfram Workbench and Eclipse and contains a collection of tools and functions for processing quantitative magnetic resonance imaging (qMRI) data. The toolbox does not provide a GUI and its primary goal is to allow for fast and batch data processing, and facilitate development and prototyping of new functions. The core of the toolbox contains various functions for data manipulation and restructuring.

The toolbox was developed in the context of quantitative muscle, nerve and cardiac magnetic resonance imaging. The library of functions grows along with the research it is used for and started as a toolbox to analyze diffusion weighted imaging (DWI) data of muscle (M. Froeling et al., 2012). Although there exist many different software packages and code repositories for much of the functionality in this toolbox, I was in need of one that did all. Furthermore, most diffusion packages are optimized for brain analysis and provide limited flexibility. QMRTTools works alongside other software packages (e.g., [vIST/e](#), and [ITKSnap](#)) and for some functionality it calls external executables (e.g. [dcm2nii](#) and [Elastix](#)). The toolbox has been used in various studies [e.g. M. Froeling et al. (2012); Hooijmans et al. (2015); M. Froeling et al. (2015); [Froeling2015a](#)].

The toolbox includes some [demo data](#) that is used in the demo file `demo.nb`. In this notebook, most of the functionality of the toolbox is demonstrated. A full list of functions and packages can be found in the [file All-Functions.nb](#) (also available as [pdf](#)). For all functions and toolboxes, help files and guides are available and the documentation is built using workbench making it available in the Wolfram documentation.

The toolbox contains some basic functionality such as DICOM and Nifti import, and 2D, 3D and 4D data visualization. The advanced features comprise data registration (Klein, Starling, Murphy, Viergever, & Pluim, 2010; Shamonin, 2013), noise suppression (Aja-Fernandez, Niethammer, Kubicki, Shenton, & Westin, 2008; Veraart, Fieremans, & Novikov, 2016a), diffusion drift correction (Vos et al., 2017), gradient direction optimization (M. Froeling, Tax, Vos, Luijten, & Leemans, 2017), simulation framework (M. Froeling, Nederveen, Nicolay, & Strijkers, 2013), extended phase graph (EPG) based T2 fitting (Marty et al., 2016; Weigel, 2015) and iterative decomposition of water and fat with echo asymmetry and least-squares estimation (IDEAL) Dixon reconstruction (Herraez, Burton, Lalor, & Gdeisat, 2002; Reeder et al., 2005). The current functional toolboxes with a short description are listed below.

## Toolboxes

### Cardiac Tools

A collection of tools to analyze cardiac data. The main features are cardiac shape analysis that defines the heart in a local myocardial coordinate system which allows quantifying and

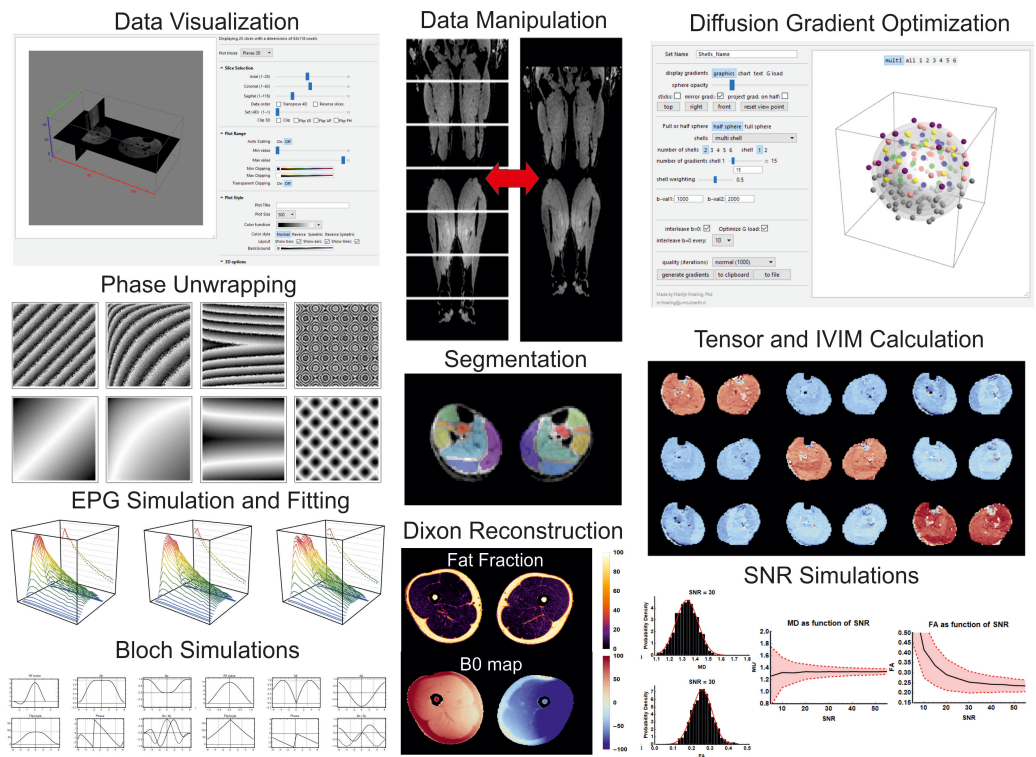


**Figure 1:** An overview of some of the functionality in the QMRTTools Mathematica add-on.

analyzing data. When the cardiac geometry is known there are functions to analyze qMRI parameters in the AH17 model (Cerdeira et al., 2002) or perform transmural sampling of quantitative MRI parameters. Most of the functionality is demonstrated in the `demo.nb`.

## CoilTools

A collection of tools to evaluate complex multi-coil data. The functions are specific for analysis of multi-coil magnitude and noise data which allows quantifying per channel signal to noise ratio (SNR). Furthermore, if complex coil sensitivity maps are available it allows performing SENSE g-factor maps simulations.

This toolbox is not demonstrated in the `demo.nb`.

## DenoiseTools

The toolbox provides two algorithms that allow denoising of DWI data. The first is based on and linear minimum mean square error (LMMSE) framework (Aja-Fernandez et al., 2008), the second is based on a random matrix theory and Principal component analysis framework (Veraart et al., 2016a, 2016b). Furthermore, it provides an anisotropic filter for denoising the estimated diffusion tensor which provides more reliable fiber orientation analysis (Lee, Chung, & Alexander, 2006). Most of the functionality is demonstrated in the `demo.nb`.

## DixonTools

An iterative decomposition of water and fat with echo asymmetry and least-squares estimation (IDEAL) based Dixon reconstruction algorithm (Reeder et al., 2005; Yu et al., 2008). The

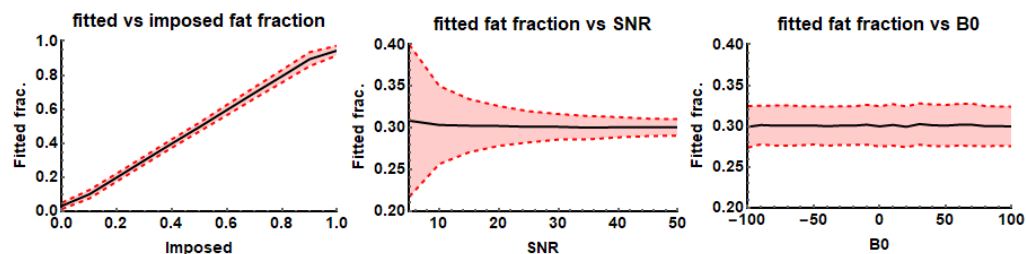


**Figure 2:** IDEAL based Dixon reconstruction: fitted fat fractions as a function of the imposed fat fraction, SNR and B0 field offset.

method provides multi-peak fitting B0 field and T2\* correction. The toolbox also provides a function for unwrapping phase data in 2D and 3D based on a best path method (Abdul-Rahman et al., 2007; Herraez et al., 2002). It also contains a function that allows simulating gradient echo Dixon data. Most of the functionality is demonstrated in the `demo.nb`.

## ElastixTools

A wrapper that calls the Elastix registration framework (Klein et al., 2010; Shamonin, 2013). The toolbox determines what registration or transformations need to be performed, exports the related data to a temp folder and calls an automatically generated command line script that performs the registration. After registration is completed the data is again loaded into Mathematica. Most of the functionality is demonstrated in the `demo.nb`.

## GeneralTools

This toolbox provides core functions used in many other functions and features. The functions comprise amongst others: data cropping, mathematical and statistical operators that ignore zero values, and data rescaling, transformation and padding. Most of the functionality is demonstrated in the `demo.nb`.

## GradientTools

The main feature is an algorithm that uses static repulsion (M. Froeling et al., 2017; Jones, Horsfield, & Simmons, 1999) to generate homogeneously distributed gradient directions for DWI experiments. It also provides functions to convert bval and bvec files to bmatrix and vice versa. Most of the functionality is demonstrated in the `demo.nb`.

## ImportTools

Allows importing Dicom data or Dicom header attributes. These functions are rarely used since the toolbox mostly uses the NIfTI data format and provides tools to convert Dicom to NIfTI via `dcm2nii`. This toolbox is not demonstrated in the `demo.nb`.

## IVIMTools

The toolbox includes functions to perform intra voxel incoherent motion (IVIM) fitting of diffusion weighted imaging (DWI) data. There are two main functions: non linear fitting and Bayesian fitting (Orton, Collins, Koh, & Leach, 2014). Some of the functionality is demonstrated in the `demo.nb`.

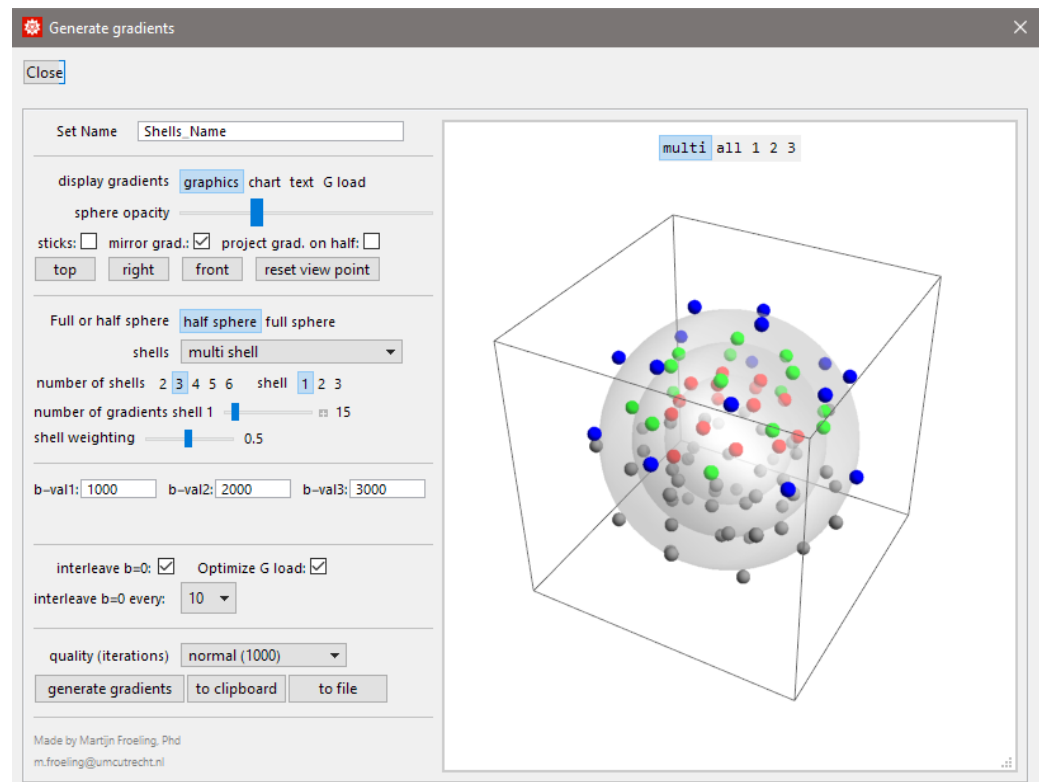


**Figure 3:** The graphical user interface of the gradient generation tool.

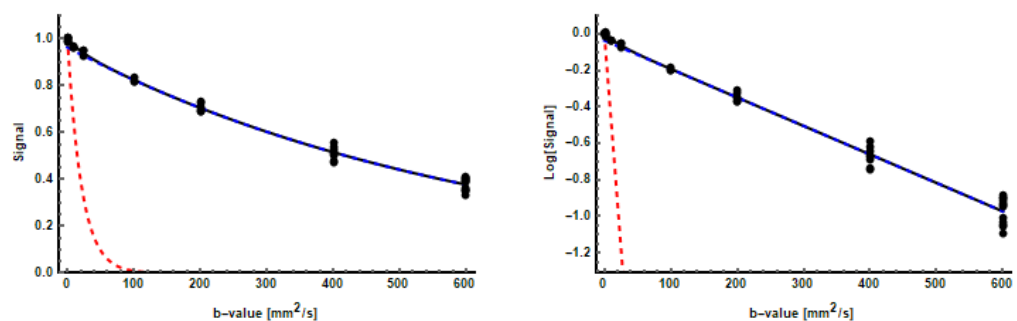


**Figure 4:** Visualization of IVIM fitting.

## JcouplingTools

A toolbox that allows simulation of NMR spectra using Hamiltonians based on methods from [FID-A](#). It allows simulating large spin systems (Castillo, Patiny, & Wist, 2011) and was mainly implemented to investigate fat spectra in multi echo spin echo acquisition (Stokes, Feng, Mitropoulos, & Warren, 2013). Most of the functionality is demonstrated in the `demo.nb`.

## MaskingTools

Tools for masking and homogenization of data. It provides functions for smoothing cutting and merging masks and functions for the evaluation of data within masks. Most of the functionality is demonstrated in the `demo.nb`.

## NiftiTools

Import and export of the NIfTI file format. Part of the code is based on previously implemented [nii-converter](#). For converting DICOM data to the NIfTI file format the toolbox uses [dcm2niix](#). It also provides some specialized NIfTI import functions for specific experiments which are probably not generalizable. Most of the functionality is demonstrated in the `demo.nb`.

## PhysiologyTools

Functions for importing and analyzing Philips physiology logging and RespirAct trace files. The functions are rarely used and not well supported. This toolbox is not demonstrated in the `demo.nb`.

## PlottingTools

A variety of functions for visualization of various data types. The main functions are 'PlotData' and 'PlotData3D' which allow viewing 2D, 3D and 4D data. Most of the functionality is demonstrated in the `demo.nb`.

## ProcessingTools

The toolbox comprises a variety of functions that allow data manipulation and analysis. The main functions allow joining multiple data sets into one continuous data set (M. Froeling et al., 2015) or to split data of two legs into two separate data-sets. Furthermore, it contains a collection of functions for data evaluation and analysis. Most of the functionality is demonstrated in the `demo.nb`.

## RelaxometryTools

A collection of tools to fit T2, T2\*, T1rho and T1 relaxometry data. The main function of this toolbox is an extended phase graph (EPG) (Weigel, 2015) method for multi-compartment T2 fitting of multi-echo spin echo data (Marty et al., 2016). Therefore it provides functions to simulate and evaluate EPG. Some of the functionality is demonstrated in the `demo.nb`.

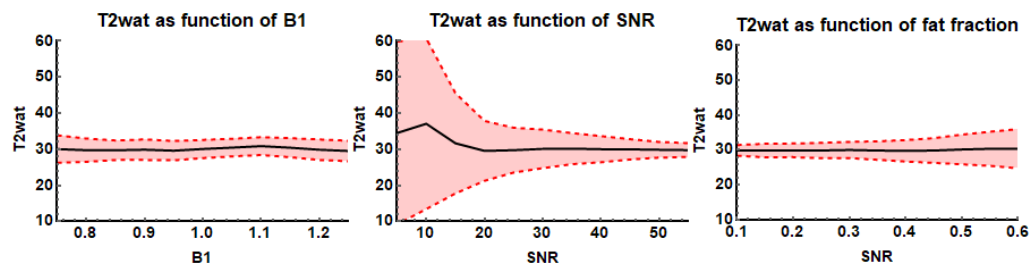


**Figure 5:** Demonstration of EPG based T2 fitting: the fitted water T2 relaxation as a function of B1, SNR and fat fraction.

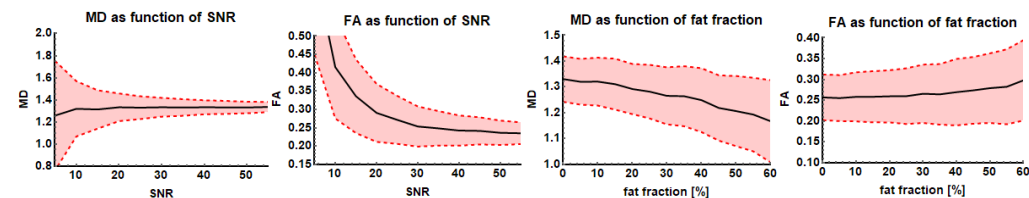


**Figure 6:** MD and FA as a function of SNR and fat fraction. Results are from simulated data using an iWLLS algorithm with outlier rejection.

## Simulation Tools

The main purpose of this toolbox is to simulate diffusion tensor imaging (DTI) based DWI data and contains some functions to easily perform analysis of the fit results of the simulated signals (M. Froeling et al., 2013). Some of the functionality is demonstrated in the `demo.nb`.

## Tensor Tools

The original toolbox where the project started. The main functions in this toolbox are to fit and evaluate the diffusion tensor model. Various fitting methods are implemented (e.g. LLS, NLS, WLLS, and iWLLS). The default method is an iterative weighted linear least squares approach (Veraart, Sijbers, Sunaert, Leemans, & Jeurissen, 2013). The tensor fitting also includes outlier detections using REKINDLE (C. M. Tax, Otte, Viergever, Dijkhuizen, & Leemans, 2015) and data preparation includes drift correction (Vos et al., 2017). Most of the functionality is demonstrated in the `demo.nb`.

## Viste Tools

Import and export functions for tensor data which can be used in the `vIST/e` tractography tool. None of the functionality is demonstrated in the `demo.nb`.

## References

Abdul-Rahman, H. S., Gdeisat, M. A., Burton, D. R., Lalor, M. J., Lilley, F., & Moore, C. J. (2007). Fast and robust three-dimensional best path phase unwrapping algorithm. *Applied Optics*, 46(26), 6623. doi:[10.1364/AO.46.006623](https://doi.org/10.1364/AO.46.006623)

Aja-Fernandez, S., Niethammer, M., Kubicki, M., Shenton, M. E., & Westin, C. F. (2008). Restoration of DWI data using a rician LMMSE estimator. *IEEE Transactions on Medical Imaging*, 27(10), 1389–1403. doi:[10.1109/TMI.2008.920609](https://doi.org/10.1109/TMI.2008.920609)

- Castillo, A. M., Patiny, L., & Wist, J. (2011). Fast and accurate algorithm for the simulation of NMR spectra of large spin systems. *Journal of Magnetic Resonance*, 209(2), 123–130. doi:[10.1016/j.jmr.2010.12.008](https://doi.org/10.1016/j.jmr.2010.12.008)
- Cerqueira, M. D., Weissman, N. J., Dilsizian, V., Jacobs, A. K., Kaul, S., Laskey, W. K., Pennell, D. J., et al. (2002). Standardized myocardial segmentation and nomenclature for tomographic imaging of the heart: A Statement for Healthcare Professionals from the Cardiac Imaging Committee of the Council on Clinical Cardiology of the American Heart Association. *Circulation*, 105(4), 539–542. doi:[10.1161/hc0402.102975](https://doi.org/10.1161/hc0402.102975)
- Froeling, M., Nederveen, A. J., Heijtel, D. F. R., Lataster, A., Bos, C., Nicolay, K., Maas, M., et al. (2012). Diffusion-tensor MRI reveals the complex muscle architecture of the human forearm. *Journal of Magnetic Resonance Imaging*, 36(1), 237–248. doi:[10.1002/jmri.23608](https://doi.org/10.1002/jmri.23608)
- Froeling, M., Nederveen, A. J., Nicolay, K., & Strijkers, G. J. (2013). DTI of human skeletal muscle: The effects of diffusion encoding parameters, signal-to-noise ratio and T2 on tensor indices and fiber tracts. *NMR in Biomedicine*, 26(11), 1339–1352. doi:[10.1002/nbm.2959](https://doi.org/10.1002/nbm.2959)
- Froeling, M., Oudeman, J., Strijkers, G. J. G. J., Maas, M., Drost, M. R. M. R., Nicolay, K., & Nederveen, A. J. A. J. (2015). Muscle Changes Detected with Diffusion-Tensor Imaging after Long-Distance Running. *Radiology*, 274(2), 548–562. doi:[10.1148/radiol.14140702](https://doi.org/10.1148/radiol.14140702)
- Froeling, M., Strijkers, G. J., Nederveen, A. J., & Luijten, P. R. (2015). Whole heart DTI using asymmetric bipolar diffusion gradients. *Journal of Cardiovascular Magnetic Resonance*, 17(Suppl 1), 1–2. doi:[10.1186/1532-429X-17-S1-P15](https://doi.org/10.1186/1532-429X-17-S1-P15)
- Froeling, M., Tax, C. M. W., Vos, S. B., Luijten, P. R., & Leemans, A. (2017). MASSIVE brain dataset: Multiple acquisitions for standardization of structural imaging validation and evaluation. *Magnetic Resonance in Medicine*, 77(5), 1797–1809. doi:[10.1002/mrm.26259](https://doi.org/10.1002/mrm.26259)
- Herraez, M. A., Burton, D. R., Lalor, M. J., & Gdeisat, M. A. (2002). Fast two-dimensional phase-unwrapping algorithm based on sorting by reliability following a noncontinuous path. *Applied Optics*, 41(35), 7437. doi:[10.1364/AO.41.007437](https://doi.org/10.1364/AO.41.007437)
- Hooijmans, M. T., Damon, B. M., Froeling, M., Versluis, M. J., Burakiewicz, J., Verschueren, J. J. G. M., Niks, E. H., et al. (2015). Evaluation of skeletal muscle DTI in patients with duchenne muscular dystrophy. *NMR in Biomedicine*, 28(11), 1589–1597. doi:[10.1002/nbm.3427](https://doi.org/10.1002/nbm.3427)
- Jones, D. K., Horsfield, M. A., & Simmons, A. (1999). Optimal strategies for measuring diffusion in anisotropic systems by magnetic resonance imaging. *Magnetic Resonance in Medicine*, 42(3), 515–525. doi:[10.1002/\(SICI\)1522-2594\(199909\)42:3<515::AID-MRM14>3.0.CO;2-Q](https://doi.org/10.1002/(SICI)1522-2594(199909)42:3<515::AID-MRM14>3.0.CO;2-Q)
- Klein, S., Staring, M., Murphy, K., Viergever, M. A., & Pluim, J. P. W. (2010). Elastix: A toolbox for intensity-based medical image registration. *IEEE Transactions on Medical Imaging*, 29(1), 196–205. doi:[10.1109/TMI.2009.2035616](https://doi.org/10.1109/TMI.2009.2035616)
- Lee, J. E., Chung, M. K., & Alexander, A. L. (2006). Evaluation of Anisotropic Filters for Diffusion Tensor Imaging. In *3rd ieee international symposium on biomedical imaging* (pp. 77–80). IEEE. doi:[10.1109/ISBI.2006.1624856](https://doi.org/10.1109/ISBI.2006.1624856)
- Marty, B., Baudin, P. Y., Reyngoudt, H., Azzabou, N., Araujo, E. C. A., Carlier, P. G., & Sousa, P. L. de. (2016). Simultaneous muscle water T2and fat fraction mapping using transverse relaxometry with stimulated echo compensation. *NMR in Biomedicine*, 29(4), 431–443. doi:[10.1002/nbm.3459](https://doi.org/10.1002/nbm.3459)
- Orton, M. R., Collins, D. J., Koh, D.-M., & Leach, M. O. (2014). Improved intravoxel incoherent motion analysis of diffusion weighted imaging by data driven Bayesian modeling. *Magnetic Resonance in Medicine*, 71(1), 411–420. doi:[10.1002/mrm.24649](https://doi.org/10.1002/mrm.24649)

- Reeder, S. B., Pineda, A. R., Wen, Z., Shimakawa, A., Yu, H., Brittain, J. H., Gold, G. E., et al. (2005). Iterative decomposition of water and fat with echo asymmetry and least-squares estimation (IDEAL): Application with fast spin-echo imaging. *Magnetic Resonance in Medicine*, 54(3), 636–644. doi:[10.1002/mrm.20624](https://doi.org/10.1002/mrm.20624)
- Shamonin, D. (2013). Fast parallel image registration on CPU and GPU for diagnostic classification of Alzheimer's disease. *Frontiers in Neuroinformatics*, 7(January), 50. doi:[10.3389/fninf.2013.00050](https://doi.org/10.3389/fninf.2013.00050)
- Stokes, A. M., Feng, Y., Mitropoulos, T., & Warren, W. S. (2013). Enhanced refocusing of fat signals using optimized multipulse echo sequences. *Magnetic Resonance in Medicine*, 69(4), 1044–1055. doi:[10.1002/mrm.24340](https://doi.org/10.1002/mrm.24340)
- Tax, C. M., Otte, W. M., Viergever, M. A., Dijkhuizen, R. M., & Leemans, A. (2015). REKINDLE: Robust Extraction of Kurtosis INDices with Linear Estimation. *Magnetic Resonance in Medicine*, 73(2), 794–808. doi:[10.1002/mrm.25165](https://doi.org/10.1002/mrm.25165)
- Veraart, J., Fieremans, E., & Novikov, D. S. (2016a). Diffusion MRI noise mapping using random matrix theory. *Magnetic Resonance in Medicine*, 76(5), 1582–1593. doi:[10.1002/mrm.26059](https://doi.org/10.1002/mrm.26059)
- Veraart, J., Novikov, D. S., Christiaens, D., Ades-aron, B., Sijbers, J., & Fieremans, E. (2016b). Denoising of diffusion MRI using random matrix theory. *NeuroImage*, 142, 394–406. doi:[10.1016/j.neuroimage.2016.08.016](https://doi.org/10.1016/j.neuroimage.2016.08.016)
- Veraart, J., Sijbers, J., Sunaert, S., Leemans, A., & Jeurissen, B. (2013). Weighted linear least squares estimation of diffusion MRI parameters: Strengths, limitations, and pitfalls. *NeuroImage*, 81, 335–346. doi:[10.1016/j.neuroimage.2013.05.028](https://doi.org/10.1016/j.neuroimage.2013.05.028)
- Vos, S. B., Tax, C. M. W., Luijten, P. R., Ourselin, S., Leemans, A., & Froeling, M. (2017). The importance of correcting for signal drift in diffusion MRI. *Magnetic Resonance in Medicine*, 77(1), 285–299. doi:[10.1002/mrm.26124](https://doi.org/10.1002/mrm.26124)
- Weigel, M. (2015). Extended phase graphs: Dephasing, RF pulses, and echoes - pure and simple. *Journal of Magnetic Resonance Imaging*, 41(2), 266–295. doi:[10.1002/jmri.24619](https://doi.org/10.1002/jmri.24619)
- Yu, H., Shimakawa, A., McKenzie, C. A., Brodsky, E., Brittain, J. H., & Reeder, S. B. (2008). Multiecho water-fat separation and simultaneous R<sup>2</sup> estimation with multifrequency fat spectrum modeling. *Magnetic Resonance in Medicine*, 60(5), 1122–1134. doi:[10.1002/mrm.21737](https://doi.org/10.1002/mrm.21737)